IEEE Access
Multidisciplinary | Rapid Review | Open Access Journal

IEEE POWER & ENERGY SOCIETY SECTION

Received 4 April 2023, accepted 5 May 2023, date of publication 10 May 2023, date of current version 17 May 2023.

Digital Object Identifier 10.1109/ACCESS.2023.3274738

RESEARCH ARTICLE

Optimal Net Load Flattening in Unbalanced Distribution Systems via Rank-Penalized Semidefinite Programming

IBRAHIM ALSALEH[1], (Member, IEEE), HAMOUD ALAFNAN[1], ABDULLAH ALASSAF[1], AND ANAS ALMUNIF[2], (Member, IEEE)

[1]Department of Electrical Engineering, College of Engineering, University of Hail, Hail 81441, Saudi Arabia
[2]Department of Electrical Engineering, College of Engineering, Majmaah University, Al Majma'ah 11952, Saudi Arabia

Corresponding author: Ibrahim Alsaleh (i.alsaleh@uoh.edu.sa)

This work was supported by the Scientific Research Deanship, University of Hail, Saudi Arabia, under Project BA-2110.

ABSTRACT A formidable challenge that hinders the widespread adoption of renewable energy sources is the potential mismatch between their intermittent supply and the fluctuating demand. This necessitates proper coordination to moderate temporal net load variations while reducing costly curtailment of renewable energy production. By capturing the physical and security constraints of unbalanced distribution systems, this paper formulates a problem to manage various fleets of commercial- and residential-scale distributed energy resources (DERs), i.e., photovoltaics (PVs), deferrable loads (DLs), electric vehicles (EVs), and thermostatically-controlled loads (TCLs). A multi-phase distribution system expanded on the relaxed power flow constraints is considered to account for network awareness. The proposed objective is to minimize hour-to-hour fluctuations of the net load variable, reduce solar energy curtailment, and prioritize preferred EV state of charge and indoor temperature. This objective, however, renders the convex relaxation inexact, wherein positive-semidefinite (PSD) matrices are higher than rank-1. To overcome this issue and therefore enhance the reliability of the solution, we propose to tighten the relaxation constraints via appending the trace of the power flow PSD matrices to the objective function. Multiple case studies on the IEEE 13-bus feeder demonstrate the effectiveness of the proposed problem to optimize the load profile and yield exact solutions.

INDEX TERMS Multi-objective optimization, net load flattening, unbalanced distribution systems, penalized semidefinite programming.

I. INTRODUCTION

Electricity has become an indispensable part of modern society, powering various equipment and appliances, including vehicles, heating/cooling systems, and smart devices. The escalating consumption of these devices, spanning residential and commercial sectors, coupled with the accelerated integration of distributed energy resources (DERs) has reshaped the dynamics of distribution systems. The reliance on fossil fuel-based synchronous generators (SGs) to address the fluctuations in net demand is no longer a viable option given the substantial environmental consequences. Driven by the quest for sustainability, governments worldwide are actively promoting the use of renewables by implementing policies such as tax credits and feed-in tariffs, thereby encouraging investments in clean energy infrastructure. In light of these developments, the need for cutting-edge methodologies designed to coordinate renewables and responsive demand has become a critical research area.

The integration of renewable energy resources en masse has engendered new challenges, stemming from the intermittency and weather dependency of renewables. These factors result in significant fluctuations in the net demand, which is the difference between the total demand and the renewable generation. As illustrated in Fig. 1a, this situation could give rise to the notorious "duck curve" characterized by a steep

The associate editor coordinating the review of this manuscript and approving it for publication was Pierluigi Siano.

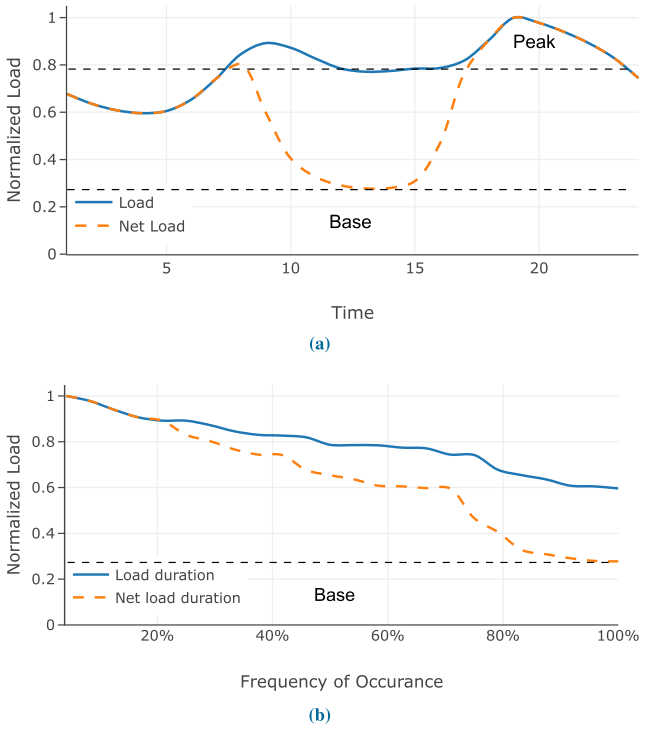

FIGURE 1. (a) An example of a load profile and a net load profile when solar penetration is 50%. It shows that, within 6 hours, the net load ramps from approximately 0.28 (13 h) to the peak load (19 h). (b) The load and net load curves for the profiles shown in (a).

decline and ascent of net load within a short time span [1], [2]. In addition to voltages potentially exceeding their limits [3], the formation of lower base loads, as shown in Fig. 1b, requires rapid ramping of conventional generation to balance supply and demand, incurring standby SG start-up expenses as well as the degradation of mechanical components. The severity of the duck curve's slope may escalate at a rate commensurate with non-curtailable renewable energy penetration, threatening the system's stability and reliability and demanding advanced methods to regulate energy flow and consumption patterns.

A. LITERATURE REVIEW

A recent work [4] introduces a distributed methodology that utilizes the thermal mass of households as an energy storage system (ESS) for flattening the duck curve through pre-cooling. The efficacy of the proposed approach is investigated via detailed simulations at the household level, while its impact is evaluated at the system level using an aggregated demand model based on probability distributions. Safdarian et al. [5] propose a distributed algorithm where flexible loads can collectively achieve a flattened load profile, while Singhal et al. [6] propose a new transactive market mechanism where electric vehicle (EV) users can opt in or out of charging during peak prices/demand based on a saving versus comfort slider. Moreover, Rezaei and AliAkbar Golkar [7] schedule plug-in EVs at a parking lot to flatten the day-ahead load. Although the methodologies in [4], [5], [6], and [7] represent a potentially effective and less infrastructure-dependent measure to flatten the duck curve, the studies fall short of examining the effect of demand response on the power flow and voltages of the power system.

DR and dispatch of renewables can be effectively carried out by solving optimal power flow (OPF) problems. By capturing the physical and operational characteristics of the power system in a mathematical model, OPF can enhance the operation of the power system, address the challenges associated with renewable integration, and enable the participation of various grid stakeholders in the control process. The scheduling of demand and distributed generation hinges upon demand and production forecasts [8], [9]. To accomplish this, day-ahead forecasts that detail hourly figures of power demand and production are generated. Thus, considering the quasi steady-state of the power system, the distribution system operator (DSO) undertakes the task of solving an OPF problem at regular intervals [10].

In [11], a demand-side management scheme is proposed for smart grid that adapts demand elasticity in the presence of volatile generations. The paper considers households that operate different appliances including plug-in hybrid electric vehicles (PHEVs) and batteries and models their utility functions based on their preferences. The works in [12] and [13] employ a DC-linearized OPF to minimize fuel and start-up costs of thermal power plants while integrating pumped-storage hydroelectricity (PSH) and concentrated solar plants (CSPs), thereby reducing the duck curve caused by midday PV power saturation. Although the primary objective of this model is to minimize the fuel and start-up costs of thermal units, it also incidentally flattens the duck curve by mitigating the impact of midday PV power saturation. Despite this model's effectiveness, it does not address the issue of duck curve flattening directly, but rather as a byproduct of minimizing thermal unit costs. Further, DC OPF has inherent limitations that cannot be overlooked. One such limitation is that the DC approximation of power flow equations neglects losses and reactive powers, and assumes flat voltage magnitudes. Such a simplistic approximation may lead to DER dispatch solutions that defy the system's constraints, rendering them unfeasible in practice.

The utilization of alternating current OPF (AC OPF) has proven to be paramount to adherence to system constraints. As demand response and renewable control take place in distribution systems, it is vital that the associated constraints of these systems are considered. Reference [14] aims to minimize the line losses and maximize social welfare in distribution systems by adjusting the demand of each household according to their preferences and constraints. The problem is outlined for single-phase systems, which may fail to capture the full range of unbalanced distribution systems. In addition, Shi et al. [14] contend that maximizing the utilities of the electric equipment may create a new demand peak if the parameters are not chosen carefully, which could undermine the benefits of the demand response. Chen et al. [15]

incorporate an unbalanced distribution system and propose a method to estimate the range of net power injection at the substation achievable through the coordination of photovoltaics (PVs) and responsive demand, utilizing an optimization problem that improves upon the linearization of power flow presented in [16].

The principal goal of this paper is to address the intricate challenge of minimizing day-ahead net load fluctuations while optimizing user-defined consumption and reducing solar power curtailment. We approach this complex issue by leveraging the coordination of flexible loads in distribution networks, which involve an array of distributed energy generators, including energy-constrained deferrable demand (DLs), photovoltaic (PV) systems paired with battery energy storage systems (BESSs), electric vehicles (EVs), and thermostatically-controlled loads (TCLs). By integrating these diverse components and devising a coordinated optimization strategy, we aim to significantly enhance the efficiency and effectiveness of the energy management process. We utilize the potential of multiphase ACOPF to efficiently capture the interplay of demand and distributed generation across nodes and phases in distribution systems. We also recognize the inherent trade-off involved in the utility maximization approach and the possibility of generating a paradoxical DR peak that may undermine its effectiveness. In response, we propose an objective function to schedule the various responsive loads to flatten the net demand. By minimizing the inter-temporal net load function, we aim to reduce both peak load and load variability, which are important factors for grid stability and efficiency.

B. RANK MINIMIZATION IN ACOPF PROBLEMS

In this study, we encounter an inexact convex relaxation due to the higher rank of the positive-semidefinite (PSD) matrices arising from the proposed objective function, which is a common occurrence for a wide range of convex ACOPF problems that optimize objectives beyond the conventional loss and generation minimization [17], [18], [19], [20]. The literature offers various methods to tackle rank deviation and tighten the SDP relaxation in ACOPF problems, such as the difference of convex approach [17] and convex iteration [20], [21].

The rank-1 constraint is a crucial component of the optimization problem, as its removal can lead to infeasibility with respect to the original problem. Specifically, if the rank of all PSD matrices is not 1, the projected solution may lie outside the feasible region and fail to satisfy the desired objectives. Objective functions aimed at achieving desired voltage levels have also been shown to lead to infeasible solutions in previous research [17], [20], [22].

The literature presents several methods to address rank deviation and tighten the SDP relaxation in the context of ACOPF problems. For instance, Wei et al. [17] propose a sequential convex optimization method that restores solution feasibility by decomposing the ACOPF problem into a second-order cone inequality and a non-convex constraint

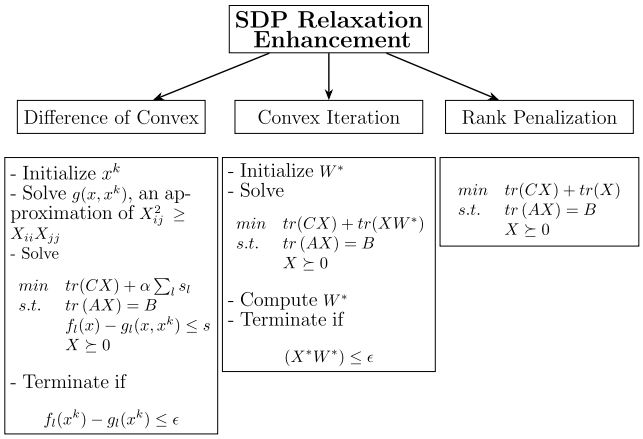

FIGURE 2. Succinct formulations of the three techniques employed to improve the accuracy of the ACOPF SDP relaxation. The difference of convex and convex iteration approaches are iterative in nature, whereas the adopted rank relaxation technique is non-iterative, making it well-suited for multi-time energy-constrained ACOPF problems.

involving the difference of two convex functions. Referred to as the difference of convex approach, this method linearizes the concave constraint and sequentially tightens the relaxation. In another approach, Alsaleh et al. [20] and Wang and Yu [21] employ another iterative method, called convex iteration, wherein a regularization term is appended to the objective function to minimize the inferior eigenvalues (and maximize the superior eigenvalue) [23]. The stopping criteria in these works differ; while [20] relies on the exactness of the PSD matrices, [21] depends on the diminishment of the regularization term. However, both techniques—the difference of convex and convex iteration—require solving the SDP problems multiple times, as highlighted in Fig. 2, making them unsuitable for multi-time energy-constrained ACOPF problems due to their iterative nature.

Another approach is based on penalizing the trace of the PSD matrix so as to minimize the inferior eigenvalues that cause the rank to be more than 1. Previously, the method was used to recover feasible solutions for single-phase transmission-level ACOPF problems [24], [25], [26]. Recently, the penalization method was adopted by [27] for the multi-phase distribution-level ACOPF to incorporate the constraints of delta connections. This method offers faster computation compared to its iterative counterparts, making it a promising candidate for handling multi-objective multi-time energy-constrained ACOPF problems. However, its effectiveness in this context remains largely unexplored.

C. CONTRIBUTIONS

In this paper, we adopt the non-iterative penalization technique for the multi-time ACOPF problem and demonstrate its success in recovering feasible solutions for a set of non-conventional objective functions.

In addition to the DER models, we also integrate the relaxed gang-operated voltage regulator model into the overall problem, which necessitates the inclusion of additional SDP constraints without the need for binary

variables [28]. It is important to note that while our paper's scope does not encompass long-term planning or the adjustment of volt-var devices such as reconfiguration switches and capacitor units, the proposed approach can be extended to incorporate these aspects. We acknowledge the complexities associated with incorporating switchable devices; however, given the non-iterative nature of the rank-penalized SDP, it is possible to formulate a mixed-integer SDP problem that leverages iterative algorithms [29], [30], [31]. This approach also holds potential for addressing a wider range of optimization problems, including those that focus on the strategic allocation and integration of distributed generation resources [32].

The following summarizes the contributions proposed by this paper:

- We propose a novel model that leverages the modern infrastructure of multi-phase distribution networks, flexible loads, and PV-battery systems to optimize net load curves, thereby paving the way for efficient and sustainable energy management.
- To streamline the formulation while ensuring both computational efficiency and high modeling accuracy, we build upon the ACOPF model and incorporate additional models for deferrable loads, PV-battery systems, thermostatically-controlled loads, and electric vehicles. By exploiting the underlying sparsity and the semi-definite structure of the ACOPF, we derive a rank-relaxed semidefinite programming formulation that can efficiently handle these complex and diverse models.
- In light of the objective function aimed at mitigating net-load fluctuations, the feasibility and accuracy of the solution may suffer. To counteract this degradation, we propose integrating the rank minimization method to enforce a rank-1 constraint on the positive-semidefinite (PSD) matrices. Through our approach, we are able to obtain an optimal and feasible solution, all while preserving the physical realizability and accuracy of the solution.

This paper is structured as follows: Section II lays out the theoretical foundation by introducing the SDP-based power flow equations, formulating the DER models that incorporate energy and temperature constraints, and defining the objective functions. Section III introduces the proposed methodology for recovering feasible solutions via penalized semidefinite programming. Section IV demonstrates the effectiveness of our approach through a series of case studies conducted on the IEEE 13-bus feeder. Finally, in Section V, we summarize our findings and discuss future directions for research in this area.

II. FORMULATION OF DISTRIBUTION POWER FLOW

A. NOTATIONS

We denote sets of nodes (buses) and edges (lines) by $\mathcal{N}$ and $\mathcal{E}$, respectively. Each element can be comprised a single, two, or three transmission conductors. Note that the radiality of the distribution system satisfies $|\mathcal{E}| = |\mathcal{N} \setminus 1|$, where 1 is the index of the substation node. We use $\mathcal{N}_b \subset \mathcal{N}$ to distinguish nodes with DERs. Additionally, we introduce $\mathcal{D}$, $\mathcal{T}$, $\mathcal{P}$, and $\mathcal{V}$ to denote the sets of deferrable loads, thermostatically-controlled loads, photovoltaics, and electric vehicles. Thus, the aggregate set of physical nodes is

$$\mathcal{N}_b = \mathcal{D} \cup \mathcal{T} \cup \mathcal{P} \cup \mathcal{V}$$

We define the phase sets as $\Phi = \{a, b, c\}$, $\Phi' = \{b, c, a\}$. The voltage at the substation bus, $i = 1$, is a fixed phasor vector, where magnitudes are 1 pu and phase angles are 120° apart. The voltage and current vectors are complex and defined as w_i and I_{ik}. Due to mutual coupling, the line impedance is 3×3 matrix, denoted as z_{ik}. Impedance entries whose indices belong to missing lines are replaced by zeros.

Let $s_i = \left[s_i^a, s_i^b, s_i^c\right]^T$ a vector of net demand (production minus consumption) at each bus. For example, an entry of a net-demand vector is composed of $(s_{i,d}^{\phi} - s_{i,g}^{\phi})$, where g and d denote the DER and demand complex powers.

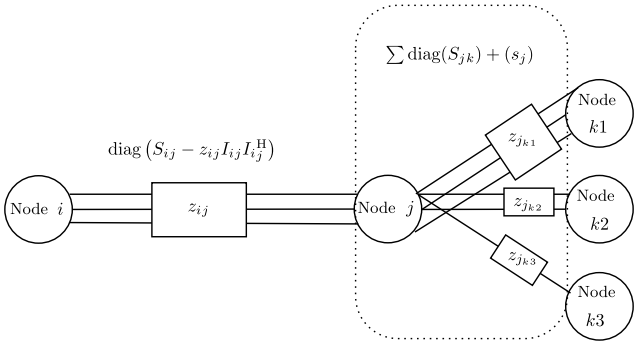

FIGURE 3. Illustration of the power balance on the power balance for line (i, j).

B. POWER FLOW MODEL

1) POWER FLOW MODEL: NON-CONVEXITIES AND RELAXATION

The following model in (1)–(2) describes the power flow in multi-phase systems:

$$W_j = W_i - z_{ij} I_{ij} \tag{1}$$

$$\mathrm{diag}\left(W_j\Big(\sum_{(j,k)\in\mathcal{L}} I_{jk}^H + I_j^H\Big)\right) = \mathrm{diag}\left(W_i I_{ij}^H - z_{ij} I_{ij} I_{ij}^H\right) \tag{2}$$

Equation (1) is the voltage drop on line (i, j), where the complex vectors of the node voltages and the line current are respectively denoted as W_i, W_j, and I_{ij}. Equation (2) is the power flow from node i to node j. Note that the equation (2) is a result of multiplying I_{ij}^H by both sides, where the left hand side is the product $W_j I_{ij}^H$, decomposed into downstream power flows on line (j, k) and net-load power at node j. The power balance equation, (2), can be re-written in terms of

complex power variables as:

$$\sum_{(j,k)\in\mathcal{E}} \text{diag}(S_{jk}) + s_j = \text{diag}(S_{ij} - z_{ij} I_{ij} I_{ij}^H) \quad \forall (i,j) \in \mathcal{E} \quad (3)$$

Fig. 3 is a depiction of the power balance for line (i, j), where node j can be any combination of three-, two-, or single-phase lines.

In order to close the loop on the power flow constraints in (1)-(2), complex power variables in (3) must be constrained as functions of voltages and currents.

$$S_{ij} = W_j I_{ij}^H \quad \forall (i,j) \in \mathcal{E} \quad (4)$$

While the previous constraints comprehensively describe the power flow, they are non-linear due to the complex variable products in (3) and (4), repeated for each line. This non-linearity hinders the computational tractability and cannot certify global optimality.

2) LIFTED POWER FLOW MODEL AND RELAXATION

In order to reduce the number of non-convex constraints and therefore obtain a nearly-convex problem, reference [33] proposed to lift the voltage and current variables, where new variables are defined as $w_i = W_i W_i^H$ and $\ell_{ij} = I_{ij} I_{ij}^H$. Hence, the voltage drop and power balance constraints are expanded in (5) and (6), whereas the complex power constraint in (4) is represented by the PSD and rank-1 constraints in (7) and (8).

$$w_j = w_i - (S_{ij} z_{ij}^H + z_{ij} S_{ij}^H) + z_{ij} \ell_{ij} z_{ij}^H, \quad \forall \ (i,j) \in \mathcal{E} \quad (5)$$

$$\sum_{(j,k)\in\mathcal{E}} \text{diag}(S_{jk}) + s_j = \text{diag}(S_{ij} - z_{ij}\ell_{ij}), \quad \forall (i,j) \in \mathcal{E} \quad (6)$$

$$\begin{bmatrix} w_i & S_{ij} \\ S_{ij}^H & \ell_{ij} \end{bmatrix} \succeq 0 \qquad \forall \ (i,j) \in \mathcal{E} \quad (7)$$

$$\text{rank}\left(\begin{bmatrix} w_i & S_{ij} \\ S_{ij}^H & \ell_{ij} \end{bmatrix}\right) = 1 \qquad \forall \ (i,j) \in \mathcal{E} \quad (8)$$

3) RELAXATION AND PROJECTION

The model presented in (5)-(8) can be relaxed merely by removing the rank-1 constraint. The solution to the convex lifted model can be projected to the original model in (1) and (2) if all PSD matrices in (7) are nearly rank-1.

C. DISTRIBUTED GENERATION, RESPONSIVE LOAD, AND VOLTAGE REGULATION MODELS

1) DEFERRABLE LOADS (DLs)

The deferrable load model is power-flexible but energy-constrained, where daily consumption must meet a predetermined energy by the end of the day. The model can be represented by the following set of constraints:

$$\forall \phi \in \Phi, \quad \forall i \in \mathcal{D}:$$

$$\underline{P}_{i,h}^{d} \le \Re(s_{i,h}^{d,\phi}) \le \overline{P}_{i,h}^{d} \quad h \in \mathcal{H} \quad (9a)$$

$$\sum_{h=1}^{\mathcal{H}} \Re(s_{i,h}^{d,\phi}) = E_i^{d,\phi} \quad (9b)$$

$s_{i,h}^{d}$ is the load complex power, and $\underline{P}_{i,h}^{d,\phi}$ and $\overline{P}_{i,h}^{d,\phi}$ are the bounds of the demand response. In this paper, we only consider a percentage of the real power demand to be flexible. That said, for each $i \in \mathcal{D}$ bounds are determined based on a flexibility coefficient, F, such that $\underline{P}_{i,h}^{d,\phi} = (1-F)\Re(s_{i,h}^{d,\phi})$, $\overline{P}_{i,h}^{d,\phi} = (1+F)\Re(s_{i,h}^{d,\phi})$ and $0 < F < 1$. Therefore, the flexibility bounds differ per load, phase, and hour.

Given that the main objective is to diversify load consumption throughout the day and flatten the net load curve, load shedding where both power and energy are curtailable is not considered in this paper.

2) THERMOSTATICALLY-CONTROLLED LOADS (TCLs)

Thermostatically controllable devices are both power- and temperature-constrained. The consumer can set the desired bounds of the indoor temperature, and determine the comfortable temperature within a time range [11], [14]. The latter is attained by the objective function.

$$\forall \phi \in \Phi, \quad h \in \mathcal{H}, \quad \forall i \in \mathcal{T}:$$

$$0 \le p_{i,h}^{t,\phi} \le \overline{P}^{t} \quad (10a)$$

$$T_{i,h}^{in,\phi} = T_{i,h-1}^{in,\phi} + \beta_1 \left(T_h^{\text{out}} - T_{i,h-1}^{in,\phi}\right) + \beta_2 p_{i,h}^{t,\phi} \quad (10b)$$

$$\underline{T} \le T_{i,h}^{t,\phi} \le \underline{T} \quad (10c)$$

The TCL real power, $p_{i,h}^{t,\phi}$, is constrained in (10a), e.g. $\overline{P}^{t} = 4kW$. The indoor temperature, T_h^{in}, constraint in (10b) evolves on an hourly-basis as a function of the outdoor temperature, previous indoor temperature, and the power of the TCL. β_1 determines the thermal change with respect to outdoor temperature, which is usually decided by the thermal insulation of residential buildings. β_2 is the appliance efficiency parameter, and it is either negative for cooling or positive for heating. The initial indoor temperature at $h = 0$ is set randomly between 24 and 30 ∘C.

3) ELECTRIC VEHICLES (EVs)

We postulate the following assumptions for the EV model:

- For simplicity, we assume EVs have unified kWh capacity. Being the U.S. top-selling EV in 2021 [34], Tesla Model 3 is selected for our case studies, which has an approximate capacity of 50 kWh.
- The elapsed time needed for full-charging is assumed to be 9 hours, which is approximately the time required with 7kW EV chargers.
- EV arrival time, h_a, is randomly selected. In this paper, the bounds of the random sample are 1 and 24, in order to account for at-home tasks (working,education, etc). Also, time after departure, where EVs are not charged, is assumed to last for 10 hours before arrival time. Therefore, the departure time, h_d, at which EVs should be charged enough is 10 hours before the arrival time.
- Further, the state of charge (SOC) of the vehicle at h_a is also randomized, to account for away-from-home charging.

Practically, charging and discharging energy conversion of EV devices are characterized with some shortage of efficiency. Charging and discharging inefficiencies usually entail using separate continuous variables to render a physically realizable state of charge. Such a model requires a non-convex constraint to prevent coincident charging and discharging [35]. This constraint is, however, not essential for some objective functions [36]. To streamline the formulation and maintain the computational advantage, inefficiencies of the EV battery can be ignored [15].

$$\forall \phi \in \Phi, \quad \forall i \in \mathcal{V}:$$

$$\underline{P}^{e} \leq \Re(s_{i,h}^{e,\phi}) \leq \overline{P}^{e} \quad h \in \mathcal{H} \tag{11a}$$

$$\begin{bmatrix} S_i^e s_{i,h}^{e,\phi} \\ (s_{i,h}^{e,\phi})^C S_i^e \end{bmatrix} \succeq 0 \quad h \in \mathcal{H} \tag{11b}$$

$$E_{i,h}^{e,\phi} = E_{i,h-1}^{e,\phi} - \Delta h \Re(s_{i,h}^{e,\phi}) \quad h \in \mathcal{H} \tag{11c}$$

$$\overline{E}^{e} \leq E_{i,h}^{e,\phi} \leq \underline{E}^{e} \quad h \in \mathcal{H} \tag{11d}$$

$$E_{i,h_d}^{e,\phi} \geq E_{des} \quad h_d \in \mathcal{H} \tag{11e}$$

Equation (11a) bounds the charging/discharging variable. If vehicle-to-grid (V2G) is enabled, the PSD matrix in (11b) constrains the capacity and reactive-power availability of the inverter [30]. The inverter's capacity is imposed by Schur's complement constraint (11b), which accurately represents the nonlinear relationship $|s_{i,h}^{e,\phi}|^2 \leq (S_i^e)^2$. Otherwise, the discharging limit and reactive power are set to zero, $\underline{P}^e = 0$ and $\Im(s_{i,h}^{e,\phi}) = 0$. Equations (11c) and (11d) are state of charge and charging limits. The desired charging state prior to departure, $\overline{E}_{des}$, is enforced by constraint (11e).

4) PHOTOVOLTAICS PAIRED WITH BATTERY ENERGY STORAGE SYSTEMS (PV-BESS)

The PV and BESS are modeled as:

$$\forall \phi \in \Phi, \quad h \in \mathcal{H}, \quad \forall i \in \mathcal{P}:$$

$$\Re(s_{i,h}^{p,\phi}) = p_h^{slr} - p_{i,h}^{crt,\phi} + p_{i,h}^{btr,\phi} \tag{12a}$$

$$0 \leq p_{i,h}^{crt} \leq p_h^{slr} \tag{12b}$$

$$\underline{P}^{btr} \leq p_{i,h}^{btr,\phi} \leq \overline{P}^{btr} \tag{12c}$$

$$\begin{bmatrix} S_i^p s_{i,h}^{p,\phi} \\ (s_{i,h}^{p,\phi})^C S_i^p \end{bmatrix} \succeq 0 \tag{12d}$$

$$E_{i,h}^{btr,\phi} = E_{i,h-1}^{btr,\phi} + \Delta h \Re(s_{i,h}^{p,\phi}) \quad h \in \mathcal{H} \tag{12e}$$

$$\overline{E}^{btr} \leq E_{i,h}^{btr,\phi} \leq \underline{E}^{btr} \quad h \in \mathcal{H} \tag{12f}$$

$$E_{i,24}^{btr,\phi} = E_{i,1}^{btr,\phi} \quad h \in \mathcal{H} \tag{12g}$$

The net power injection of a PV inverter with a BESS is enforced by the equality constraint in (12a), such that p_h^{slr} is the solar real power, which is a given parameter based on historical data and changes throughout the day, $p_{i,h}^{crt,\phi}$ represents the curtailment of the power, and $p_{i,h}^{btr,\phi}$ is the BESS power, where positive values represent discharging. In (12b), $p_{i,h}^{crt,\phi}$ is upper-bounded by the solar power output, p_h^{slr}, to prevent curtailment of power in excess of the available solar resource. It is worth noting that active power curtailment, as studied in [37], can be employed to extend the allowed PV penetration in distribution systems, and the smart functions of PV inverters, such as reactive power control and voltage regulation, can further enhance the technical benefits of PV to distribution systems.

We consider an oversized, variable-PF inverter that ensures reactive power support during peak solar generation or peak discharging. Similar to (11b), the PV-BESS inverter's capacity is imposed by (12d).

The SOC of the BESS is constrained in (12e). Note that the charging and discharging real-power variable of the BESS is contrary to that of the EV.

5) VOLTAGE REGULATOR

Maintaining voltage magnitudes within prescribed security limits is of paramount importance for distribution systems. To achieve this objective, alongside continuous reactive power support provided by inverters, an autotransformer furnished with tap changers is installed at the upstream line of the distribution system. Autotransformers are employed in the optimization problem to augment the voltage profile, ensuring seamless coordination with existing distributed generation and responsive loads.

To preserve the tractability of the optimization problem, we incorporate a binary-free voltage regulator model proposed by [28]. For a voltage regulator situated on line (i, j) and providing voltage variability on the secondary circuit within maximum and minimum tap ratio bounds, the following constraints are imposed:

$$w_i - \underline{r}^2 w_j \succeq 0 \tag{13a}$$

$$-w_i + \overline{r}^2 w_j \succeq 0 \tag{13b}$$

Here, w_i and w_j denote the squared voltages at the primary and secondary circuits of the autotransformer, respectively, while $\underline{r}$ and $\overline{r}$ represent the lower and upper bounds of the voltage regulator's range.

D. OBJECTIVE FUNCTION

1) NET LOAD FLATTENING

Assuming the previous DER models are all placed at node i, the temporal net load variable is written as:

$$s_{i,h} = s_{i,h}^{d} + p_{i,h}^{t} + s_{i,h}^{e} - s_{i,h}^{p} \quad h \in \mathcal{H} \tag{14}$$

In order to schedule flexible loads, curtailment, and charging/discharging of BESS so as reduce hour-to-hour net load fluctuations, the following inter-temporal net load function is minimized.

$$F_n = \sum_{h \in \mathcal{H}} \sum_{i \in \mathcal{N}} \sum_{\phi \in \Phi} |s_{i,h}^{\phi} - s_{i,h-1}^{\phi}| \tag{15}$$

2) CONSUMER COMFORT PRIORITIZATION

TCL consumers may desire to have a certain indoor temperature. This can be achieved by minimizing the following function over $\mathcal{H}_t$, which is the time range within which consumers prefer a fixed indoor temperature, T_{des}.

$$F_{tcl} = \sum_{h\in\mathcal{H}_t}\sum_{i\in\mathcal{T}}\sum_{\phi\in\Phi} |T_{i,h}^{in,\phi} - T_{des}| \tag{16}$$

Similarly, an EV user may want to take a trip out of the selected trip hours. Hence, EV readiness during idleness can be maximized by minimizing the following term.

$$F_e = \sum_{h\in\mathcal{H}}\sum_{i\in\mathcal{V}}\sum_{\phi\in\Phi} |E_{i,h}^{e,\phi} - E_{des}| \tag{17}$$

It should be noted that maximizing EV readiness could also minimize EV participation with V2G services.

3) CURTAILMENT REDUCTION

To avoid reduction of the PV power output, the curtailment variable is reduced by minimizing the following function:

$$F_c = \sum_{h\in\mathcal{H}}\sum_{i\in\mathcal{V}}\sum_{\phi\in\Phi} p_{i,h}^{crt,\phi} \tag{18}$$

4) OVERALL PROBLEM

The optimization problem is formulated as:

$$\begin{aligned} \min \quad & \alpha_1 F_n + \alpha_2 F_t + \alpha_3 F_e + \alpha_4 F_c \\ \text{s. t.} \quad & (5)\text{-}(14) \\ & \underline{V}^2 \le w_i \le \overline{V}^2 \quad i \in \mathcal{N} \end{aligned} \tag{19}$$

where the objective function is a combination thereof, creating a trade-off between achieving a flat net load profile, comfortable consumption, and reduced curtailment. In this paper, the net load flattening is prioritized with higher values of α_1 compared to α_2, α_3 and α_4. A good practice is to select values such that $\alpha_1+\alpha_2+\alpha_3+\alpha_4 = 1$. The effect of various weight selections is discussed in the numerical results. The squared voltage variable, w_i, is limited by the security voltage limits.

III. RANK-PENALIZED PROBLEM FORMULATION

In this section, we address the challenge of obtaining feasible solutions to the multi-time ACOPF problem, caused by the multi-objective function (15)-(17), by employing a non-iterative rank penalization approach. This technique allows us to retain the physical realizability of the solutions while overcoming the limitations of the iterative methods used to tackle rank deviation in ACOPF problems. This approach not only enhances the computational efficiency but also expands the applicability of the method to a wider range of optimization problems. In what follows, we detail the foundations of the penalized SDP approach.

The 6×6 PSD matrix in (7) is defined for line (ij) as X_{ij}. The trace of X_{ij} is equal to the sum of the eigenvalues, expressed as:

$$\text{tr}(X_{ij}) = \sum_{n=1}^{6} \lambda_n \tag{20}$$

If the PSD matrix is rank-1, the trace of X_{ij} is equal to the superior eigenvalue such that:

$$\text{tr}(X_{ij}) = \lambda_1 \tag{21}$$

where λ_1 is the largest eigenvalue. Therefore, appending $\text{tr}(X)$ to the objective function minimizes the inferior eigenvalues, $\sum \lambda_n$ where $n > 1$. In this paper, we adopt this method to render PSD matrices rank-1 and enable solution retrieval.

The overall problem then becomes

$$\begin{aligned} \min \quad & \alpha_1 F_n + \alpha_2 F_t + \alpha_3 F_e + \alpha_4 F_c \\ & + \sum_{h\in\mathcal{H}}\sum_{(ij)\in\mathcal{E}} \alpha_5^{ij} \text{tr}(X_{ij,h}) \\ \text{s. t.} \quad & (5)\text{-}(14) \\ & \underline{V}^2 \le w_i \le \overline{V}^2 \quad i \in \mathcal{N} \end{aligned} \tag{22}$$

With $\alpha_5^{ij} > 0$, the rank penalization term elevates the solution to (22) to be within the feasible region. Therefore, problem (22) is a subset of the feasible space of problem (19).

Values of α_5^{ij} can be adjusted non-uniformly. This is of the essence for applications that impact particular lines. In which case, larger values of α_5^{ij} can be chosen for lines whose PSD matrices are not rank-1. In our problem, the objective functions are the source of inexactness, and hence we choose a uniform value to penalize all PSD matrices. Reference [27] found that smaller values can lead to a global optimal solution. A thorough comparison between the convex iteration and rank penalization was conducted in [38] where both methods exhibit similar results except that the latter is faster. In our case studies, we fix α_5^{ij} at 1.

IV. NUMERICAL EXPERIMENTS

In this section, we perform case studies on the modified IEEE 13-bus distribution feeder. Before delving into the case studies, we briefly describe the main steps of the proposed method, which include data collection, preprocessing, and scheduling of the DERs. Multiple load aggregators within the distribution system gather historical solar power generation data, demand profiles, and parameters of all DERs, such as battery storage and flexible loads. Subsequently, these load aggregators preprocess the data to determine the flexibility range of the deferrable loads, considering the constraints and preferences of the users. The load aggregators then pass this information to the DSO, who is responsible for scheduling the DERs, including dispatchable resources (DLs, EVs, TCLs, and PV-BESSs), by formulating and solving a multi-objective optimization problem in (22) based on the rank-penalized convex multiphase ACOPF.

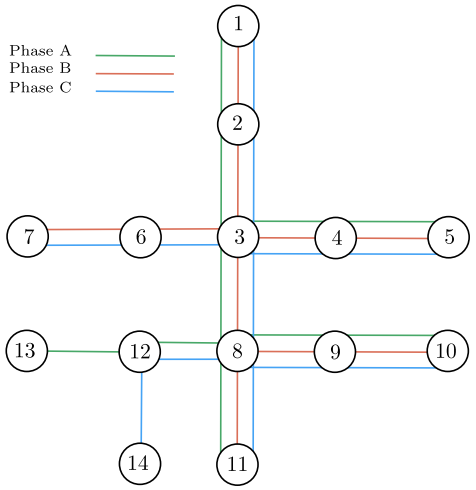

FIGURE 4. Modified IEEE 13-bus feeder.

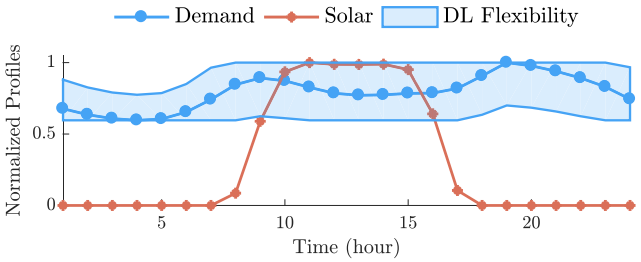

FIGURE 5. Day-ahead profiles of normalized solar irradiance and demand with DL flexibility.

A. SIMULATION SETUP

First, the problem in (22) is coded in CVX [39], [40] and solved using the commercial solver Mosek [41]. The system is unbalanced and highly loaded with a total power of 3.466 MW and 0.855 power factor. As shown in Fig. 4, the feeder exhibits dichotomy, wherein buses could be three-, two-, or single-phase. In terms of real power, loading percentages are 33.9%, 29.98%, 36.12% and respectively for phase A, B, and C. We place PVs with BESS on Bus 5, 8, 13, and 14 with uniform capacity. Thus, the solar power injection inverter is calculated as such:

$$p_{i,h}^{slr,\phi} = \eta \times \frac{\sum_{i\in\mathcal{N}} \sum_{\phi\in\Phi_i} \Re\left(s_{i,h}^{d}\right)}{|\Phi_i| \times |\mathcal{P}|}, \quad 0 < \eta < 1$$

where η is the penetration level. Note that $s_{i,h}^{d}$ alludes to the fixed real-power load. The BESS energy capability, E^{btr}, is calculated similarly, but additionally multiplied by the number of hours within which it can provide a constant power. The capacity in Table 1 is based on the assumption that BESS aggregation can provide 25% of the total load for 8 hours.

The PV-BESS inverter is sized such that it can inject solar and battery power and reactive power. Hence, an oversized inverter is used and rated in kVA as in Table 1.

Placement and parameters of EV fleets and TCL ensembles are also tabulated in Table 1. To accommodate EVs and TCLs, the original load of the feeder is reduced by 13%.

TABLE 1. Parameters and limits of flexible loads and distributed generators.

Number of DLs per bus	1
DL buses	3,5,6,7,8,9,10,11,13,14
DL Flexibility	±30%
Number of EVs per bus	5
EV buses	3,5,8,10,11
EV capacity	50kWh
EV maximum charging/discharging	±5.56 kW
EV maximum/minimum state of charge	90%/20%
Number of TCLs per bus	5
TCL buses	3,5,8,10,11
TCL maximum power consumption	4 kW
Number of PV-BESS per bus	4
PV-BESS buses	5,8,13,14
Solar penetration	50%
Single-phase inverter capacity	150 kVA
Single-phase BESS maximum charging/discharging	63 kW
Single-phase BESS energy capacity	500 kWh
Battery maximum/minimum state of charge	90%/20%

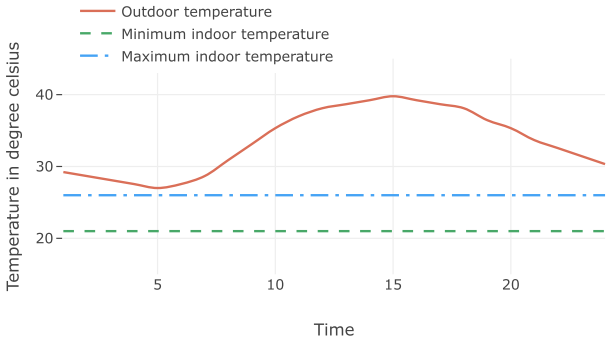

FIGURE 6. Illustration of a typical summer temperature in Saudi Arabia and desired indoor temperature bounds.

The voltage regulator is located between Bus 2 and 3 in Fig. 4. In this paper, we assume gang-operated taps with ±10% flexibility of the nominal voltage.

The variability of the demand and solar generation follows the normalized profiles depicted in Fig. 5. In the case of demand response, we assume load deferrability on all loaded buses, as tabulated in Table 1. The DL flexibility range is determined by the load aggregator based on historical load data and established demand patterns, which help identify periods of high and low demand and set the maximum and minimum bounds for deferrable load flexibility, i.e., $\overline{P}_{i,h}^{d}$ and $\underline{P}_{i,h}^{d}$. The bounds are adjusted for different times of the day to reflect consumer willingness to shift consumption, ensuring deferred consumption neither exceeds the original peak demand nor falls below the minimum original demand.

Fig. 6 shows the variations of a typical summer-day outdoor temperature along with the bounds of indoor temperature. Fig. 7 illustrates the laxity randomness of EVs.

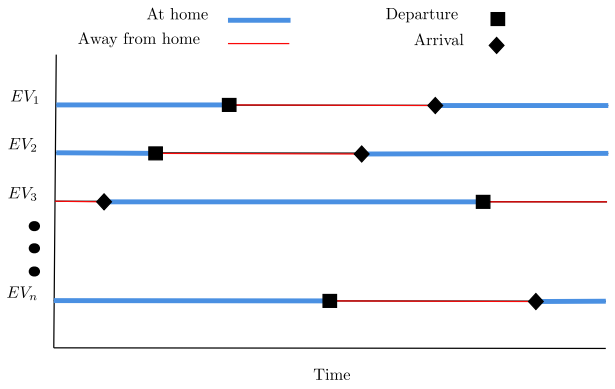

FIGURE 7. Random laxity and trip times of EVs.

We use multiple percentages to measure the effectiveness of the proposed problem to reduce curtailment and/or flatten the net load profile. The curtailment percentage, **CP**, is measured with respect to the total solar energy. **DC**, **EVC** and **TCLC** are respectively the percentages of deferred consumption of DLs, EV charging, and TCL consumption during solar generation.

B. CASE STUDIES

1) BASE CASE: WITHOUT DEMAND RESPONSE AND BATTERIES

Assuming loads are not flexible and PVs are not paired with batteries, the problem is solved with a 50% solar penetration ($\eta = 0.5$). The weights are tuned to place more importance on the load flattening objective, where $\alpha_1 = 0.5$, $\alpha_2 = 0.3$, and $\alpha_3 = \alpha_4 = 0.1$. Also, V2G capability of EVs is not active.

The temporal changes in demand, net demand, EV fleet charging, TCL ensemble consumption, and reactive power support of PV inverters are shown in Fig. 8. Fig. 8b shows that, despite the limited flexibility of EV charging and TCL consumption, the net demand is not flattened. This is mainly because EVs and TCLs are mainly governed by laxity time, temperature, and consumer preference. Phase A experiences the largest base-to-peak difference in net demand volatility when the net load increases by 766.65 kW from 2:00 PM to 7:00 PM.

The net demand is even more volatile on phase A and B due to single-phase PV configurations on bus 13 and 14, which justifies the ample Var support on phase C as depicted by Fig. 8e.

2) CASE 2: WITH DEMAND RESPONSE

We solve the problem assuming no energy storage and that loads can alter their energy consumption within the range prescribed in Fig. 5. The results in Fig. 9 show a significant improvement in the net load demand profile.

Table 2 highlights the impact of load deferrability on F_n, **CP**, **DC**, **EVC** and **TCLC**. With flexibility of load, 8.1% of total demand is deferred to midday, minimizing the total net load fluctuation by 60%. Also, Fig. 9b shows that the largest base-to-peak difference in net demand volatility dropped 62%

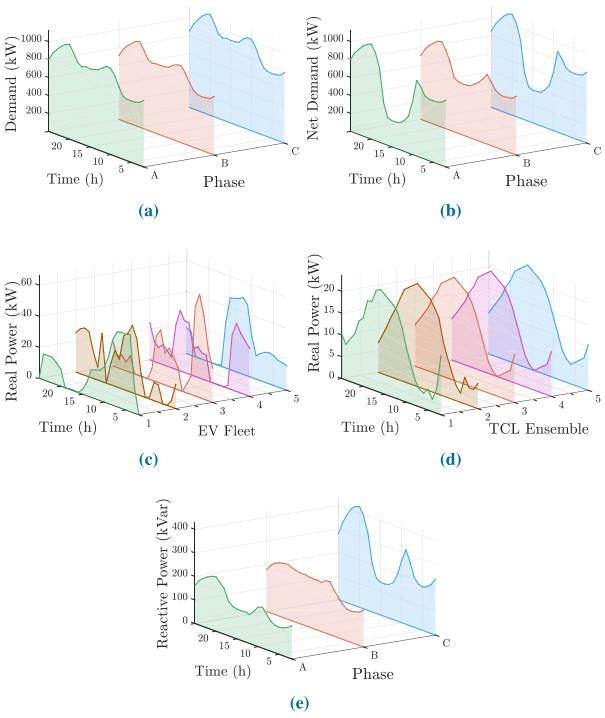

FIGURE 8. Base case: temporal changes of (a) total demand (fixed load, EVs, and TCLs), (b) net demand, (c) EV fleet consumption, (d) TCL ensemble consumption, (e) PV reactive power support. Although EV charging and TCL consumption are partially flexible, they are unable to alter the overall demand profile due to the inflexibility of the original load.

from the base case, where the net demand increases only by 290.76 kW from 2:00 PM to 7:00 PM. Interestingly, the curtailment has also reduced by approximately 49%, at the expense of a slight reduction in EV charging and TCL consumption during solar irradiance.

The impact of weight selection on net load flattening and curtailment is further investigated. Table 2 shows that without curtailment minimization, approximately 11 kWh is curtailed, amounting to 11.68% of the total solar energy, without significant change in deferred load.

On the other hand, reducing curtailment without flattening the net load results in less than 1% of curtailed solar energy. It can be concluded that, without the flattening objective, the flexible loads do not coordinate so as to mitigate the net load variability, despite the sustained load deferment. This signifies the role of the net load flattening objective.

It is clear from Fig. 8e and Fig. 9d that the PV Vars follow the net demand, preventing voltage sags during high loading.

3) CASE 3: WITH DEMAND RESPONSE AND BATTERIES

Fig. 10b shows that the net load can further improved when BESS is considered. It is noted from Fig. 10c that BESS closest to the substation consume the highest power, presumably because of their proximity to the voltage regulator, providing higher voltage levels compared to those far from the substation.

Compared to the base case, the net load fluctuation, F_n, has reduced by 69%, and curtailment has diminished to 1.46%.

TABLE 2. The trade-off between load flattening, solar energy curtailment reduction, and consumption during solar irradiance with different weight selections.

α_1	α_2	F_n	CP	DC	EVC	TCLC
Without Load Flexibility and Energy Storage						
0.5	0.3	6.35 MWh	7.46 %	43.01 %	43.04 %	57.71 %
With Load Flexibility						
0.5	0.3	2.57 MWh	3.82 %	48.03 %	40.53 %	57.68 %
0.8	0	1.99 MWh	11.68 %	47.25 %	41.03 %	57.57 %
0	0.8	4.11 MWh	0.39 %	48.74 %	39.85 %	58.08 %
With Load Flexibility and Energy Storage						
0.5	0.3	1.97 MWh	1.46 %	45.87 %	39.85 %	57.58 %
0.8	0	1.45 MWh	2.29 %	45.17 %	39.79 %	57.55 %
0	0.8	3.71 MWh	0.00 %	46.87 %	39.85 %	58.08 %

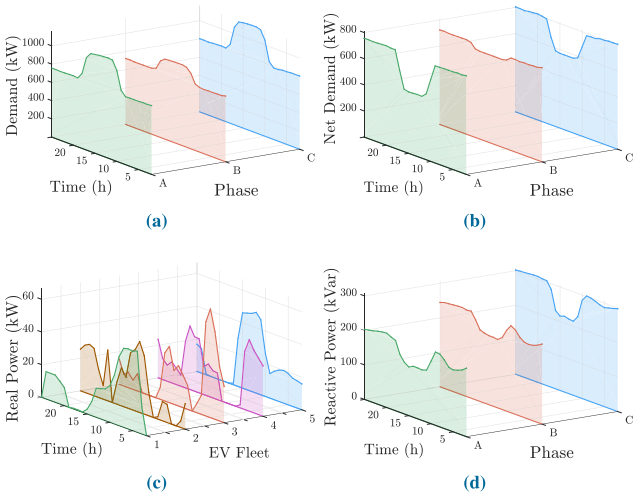

FIGURE 9. Case 2: temporal changes of (a) total demand (DLs, EVs, and TCLs), (b) net demand, (c) EV fleet consumption, (d) TCL ensemble consumption, (e) PV reactive power support. DLs have remarkably improved the net load profile. Phase B has least load and the lowest PV penetration, and thus its net load is more flattened than Phase A and B.

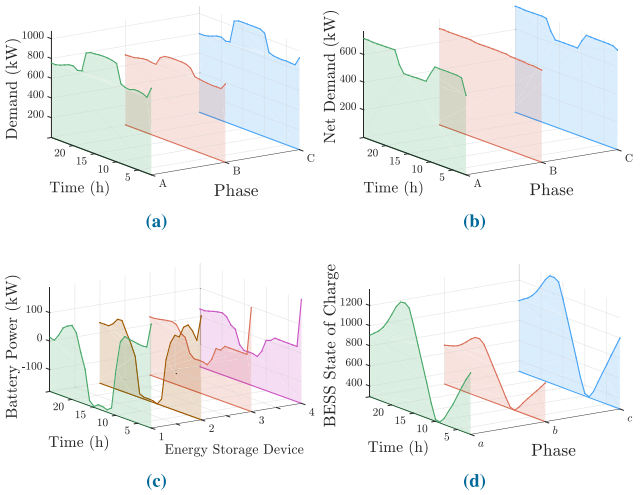

FIGURE 10. Case 3: temporal changes of (a) total demand (DLs, EVs, and TCLs), (b) net demand, (c) real power from each three-phase BESS, and (d) overall BESS state of charge. The overall demand, mainly DL consumption and BESS charging/discharging, coordinate to flatten the net load profile. The SOC shows that batteries pick up charging once solar irradiance is available.

The curtailment reduction does not seem to be affected when $\alpha_2 = 0$. On the other hand, zero curtailment is attained when $\alpha_1 = 0$, at the cost of a large net load fluctuation.

Overall, introducing load flexibility and energy storage improves the system's ability to manage net load and consumer comfort, as demonstrated by the changes in the percentage indicators (**CP**, **DC**, **EVC**, and **TCLC**). Varying the weighting factors allows us to observe the trade-offs between different objectives and select the most appropriate combination for a specific application.

In sum, it is essential to emphasize the significance of the case studies that illustrate the versatility of our rank-penalized SDP approach and its applicability to various scenarios involving optimal management of DERs while preserving physical realizability and solution accuracy. Among the presented case studies, scenarios with higher penalties on net load fluctuation are of particular importance. They demonstrate the effectiveness of our proposed multi-objective optimization approach in addressing the critical issue of harmonizing the interplay between generation and demand assets to reduce net load fluctuation.

4) CASE 4: IMPACT OF COMFORT OBJECTIVE FUNCTIONS

In the previous case studies, we solved the problem with the objective functions prioritizing the consumer's comfort for sustained EV charging and an indoor temperature of 24 °C. We examine the impact of these objectives on the EV state of charge and indoor temperature by solving the problem with $\alpha_2 = \alpha_3 = 0$.

It is evident from Fig. 11a that without the EV prioritization objective, the SOC of a single EV at Bus 3 tends to be slightly less than 90%. The temperature preference objective is more impactful, as Fig. 11b shows that the indoor temperature is kept at its maximum when α_4 is set to zero.

5) IMPACT OF α_5^U ON THE SOLUTION

The solution to the rank-relaxed (22) is deemed exact if, and only if, all PSD matrices approximate a rank-1 structure

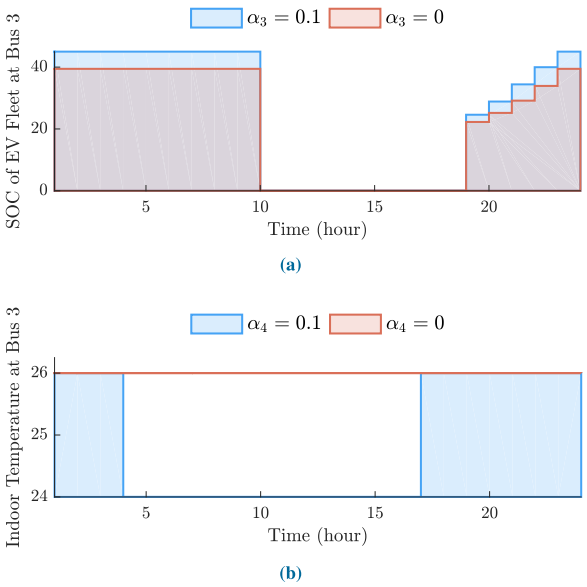

FIGURE 11. Case 4: (a) The total state of charge for EVs at Bus 3 with and without objective prioritizing 90% of charging. (b) The indoor temperature at Bus 3 with and without prioritization of 24$C°$.

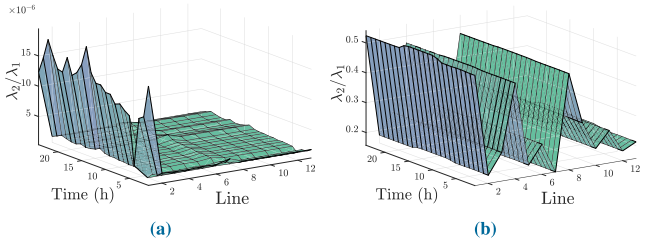

FIGURE 12. (a) Penalized rank: The ratio of the second largest eigenvalue to the largest eigenvalue for all PSD matrices. It is clear that the ratio is low, indicating the dominance of the superior eigenvalue, λ_1. (b) Without rank penalization: The ratio is large showing that the solution is inexact and therefore unreliable.

as delineated by (21). A customary method for assessing rank involves the calculation of the ratio between the second largest eigenvalue and the largest eigenvalue, denoted as λ_2/λ_1. Diminished ratios signify the preeminence of λ_1 over other eigenvalues, thereby suggesting a close approximation to the rank-1.

Upon solving case 4, the spatio-temporal ratio is computed and plotted in Fig. 12a. The maximum ratio, a minuscule 1.9468×10^{-05}, strongly indicates that the PSD matrices possess a rank-1 structure, thereby rendering the solutions feasible. To underscore the significance of rank-1 retrieval, we solve the problem without penalizing the PSD matrices, as in (19). The relatively elevated spatio-temporal ratio in Fig. 12b suggests the inexactitude of the solution, wherein the equality constraint (4) diverges considerably from being satisfied.

V. CONCLUSION

In this paper, we proposed a multi-objective optimization problem for the optimal scheduling of flexible loads and energy storage devices to achieve a flattened net load profile, reduced curtailment, and a pre-defined consumer's preference of consumption, while considering the physical constraints of a multi-phase distribution system. By leveraging the convex relaxation of the optimal power flow problem and enhancing solution quality through rank minimization, our approach demonstrates a successful coordination of various flexible loads to align peak demand with peak solar production on the IEEE 13-bus feeder. Our case studies show that energy-constrained deferrable loads have the highest contribution to net load flattening and that small-scale batteries paired with PVs can further support the achievement of our multi-objective goals.

A key strength of our work is the successful implementation of rank minimization, which renders optimal and feasible solutions to the convex ACOPF problem. This approach enables the adoption of non-conventional objective functions, paving the way for new research directions in ACOPF problem formulations.

In our future work, we will extend our current approach to develop a privacy-preserving algorithm that allows aggregators to optimize local assets while coordinating with the DSO to abide by system constraints.

REFERENCES

[1] P. Denholm, M. O'Connell, G. Brinkman, and J. Jorgenson, "Overgeneration from solar energy in California: A field guide to the duck chart," Nat. Renew. Energy Lab. (NREL), Golden, CO, USA, Tech. Rep. NREL/TP-6A20-65023, Nov. 2015.

[2] I. Alsaleh, L. Fan, and H. G. Aghamolki, "Volt/var optimization with minimum equipment operation under high PV penetration," in *Proc. North Amer. Power Symp. (NAPS)*, Sep. 2018, pp. 1–6.

[3] H. Alafnan, J. Zhao, and W. Ma, "Prevention of overvoltage induced by large penetration of photovoltaics in distribution networks by electric vehicles," in *Proc. IEEE Transp. Electrific. Conf. Expo, Asia–Pacific (ITEC Asia-Pacific)*, Jun. 2016, pp. 525–530.

[4] I. Calero, C. A. Canizares, K. Bhattacharya, and R. Baldick, "Duck-curve mitigation in power grids with high penetration of PV generation," *IEEE Trans. Smart Grid*, vol. 13, no. 1, pp. 314–329, Jan. 2021.

[5] A. Safdarian, M. Fotuhi-Firuzabad, and M. Lehtonen, "A distributed algorithm for managing residential demand response in smart grids," *IEEE Trans. Ind. Informat.*, vol. 10, no. 4, pp. 2385–2393, Nov. 2014.

[6] A. Singhal, S. Hanif, B. Bhattarai, F. B. Dos Reis, H. Reeve, and R. Pratt, "Designing a transactive electric vehicle agent with Customer's participation preference," 2022, *arXiv:2203.16516*.

[7] P. Rezaei and M. A. Golkar, "Economic load curve flattening by EVs charge and discharge scheduling in the smart grid considering machine learning-based forecasted load," in *Proc. 11th Smart Grid Conf. (SGC)*, Dec. 2021, pp. 1–5.

[8] H. Wu, M. Shahidehpour, and A. Al-Abdulwahab, "Hourly demand response in day-ahead scheduling for managing the variability of renewable energy," *IET Gener., Transmiss. Distrib.*, vol. 7, no. 3, pp. 226–234, Mar. 2013.

[9] S. S. Reddy and P. R. Bijwe, "Day-ahead and real time optimal power flow considering renewable energy resources," *Int. J. Electr. Power Energy Syst.*, vol. 82, pp. 400–408, Nov. 2016.

[10] Y. K. Renani, M. Ehsan, and M. Shahidehpour, "Optimal transactive market operations with distribution system operators," *IEEE Trans. Smart Grid*, vol. 9, no. 6, pp. 6692–6701, Jun. 2017.

[11] N. Li, L. Chen, and S. H. Low, "Optimal demand response based on utility maximization in power networks," in *Proc. IEEE Power Energy Soc. Gen. Meeting*, Mar. 2011, pp. 1–8.

[12] H. O. R. Howlader, M. M. Sediqi, A. M. Ibrahimi, and T. Senjyu, "Optimal thermal unit commitment for solving duck curve problem by introducing CSP, PSH and demand response," *IEEE Access*, vol. 6, pp. 4834–4844, 2018.

[13] H. O. R. Howlader, M. Furukakoi, H. Matayoshi, and T. Senjyu, "Duck curve problem solving strategies with thermal unit commitment by introducing pumped storage hydroelectricity & renewable energy," in *Proc. IEEE 12th Int. Conf. Power Electron. Drive Syst. (PEDS)*, Dec. 2017, pp. 502–506.

[14] W. Shi, N. Li, X. Xie, C.-C. Chu, and R. Gadh, "Optimal residential demand response in distribution networks," *IEEE J. Sel. Areas Commun.*, vol. 32, no. 7, pp. 1441–1450, Jul. 2014.

[15] X. Chen, E. Dall'Anese, C. Zhao, and N. Li, "Aggregate power flexibility in unbalanced distribution systems," *IEEE Trans. Smart Grid*, vol. 11, no. 1, pp. 258–269, Jan. 2020.

[16] A. Bernstein, C. Wang, E. Dall'Anese, J.-Y. Le Boudec, and C. Zhao, "Load flow in multiphase distribution networks: Existence, uniqueness, non-singularity and linear models," *IEEE Trans. Power Syst.*, vol. 33, no. 6, pp. 5832–5843, Nov. 2018.

[17] W. Wei, J. Wang, N. Li, and S. Mei, "Optimal power flow of radial networks and its variations: A sequential convex optimization approach," *IEEE Trans. Smart Grid*, vol. 8, no. 6, pp. 2974–2987, Nov. 2017.

[18] Q. Li and V. Vittal, "Non-iterative enhanced SDP relaxations for optimal scheduling of distributed energy storage in distribution systems," *IEEE Trans. Power Syst.*, vol. 32, no. 3, pp. 1721–1732, May 2017.

[19] N. Nazir and M. Almassalkhi, "Voltage positioning using co-optimization of controllable grid assets in radial networks," *IEEE Trans. Power Syst.*, vol. 36, no. 4, pp. 2761–2770, Jul. 2021.

[20] I. Alsaleh, L. Fan, and M. Bazrafshan, "Extended radial distribution ACOPF model: Retrieving exactness via convex iteration," *IEEE Trans. Power Syst.*, vol. 36, no. 6, pp. 4967–4978, Nov. 2021.

[21] W. Wang and N. Yu, "Chordal conversion based convex iteration algorithm for three-phase optimal power flow problems," *IEEE Trans. Power Syst.*, vol. 33, no. 2, pp. 1603–1613, Mar. 2018.

[22] S. R. Shukla, S. Paudyal, and M. R. Almassalkhi, "Efficient distribution system optimal power flow with discrete control of load tap changers," *IEEE Trans. Power Syst.*, vol. 34, no. 4, pp. 2970–2979, Jul. 2019.

[23] J. Dattorro, *Convex Optimization and Euclidean Distance Geometry*. Palo Alto, CA, USA: Meboo Publishing, 2005, pp. 306–311.

[24] R. Madani, M. Ashraphijuo, and J. Lavaei, "Promises of conic relaxation for contingency-constrained optimal power flow problem," *IEEE Trans. Power Syst.*, vol. 31, no. 2, pp. 1297–1307, Mar. 2016.

[25] R. Madani, S. Sojoudi, and J. Lavaei, "Convex relaxation for optimal power flow problem: Mesh networks," *IEEE Trans. Power Syst.*, vol. 30, no. 1, pp. 199–211, Jan. 2015.

[26] D. Molzahn, C. Josz, I. Hiskens, and P. Panciatici, "Solution of optimal power flow problems using moment relaxations augmented with objective function penalization," in *Proc. 54th IEEE Conf. Decis. Control (CDC)*, Dec. 2015, pp. 31–38.

[27] F. Zhou, A. S. Zamzam, S. H. Low, and N. D. Sidiropoulos, "Exactness of OPF relaxation on three-phase radial networks with delta connections," *IEEE Trans. Smart Grid*, vol. 12, no. 4, pp. 3232–3241, Jul. 2021.

[28] Y. Liu, J. Li, L. Wu, and T. Ortmeyer, "Chordal relaxation based ACOPF for unbalanced distribution systems with DERs and voltage regulation devices," *IEEE Trans. Power Syst.*, vol. 33, no. 1, pp. 970–984, Jan. 2018.

[29] Y. Liu, J. Li, and L. Wu, "Coordinated optimal network reconfiguration and voltage regulator/DER control for unbalanced distribution systems," *IEEE Trans. Smart Grid*, vol. 10, no. 3, pp. 2912–2922, May 2019.

[30] I. Alsaleh and L. Fan, "Multi-time co-optimization of voltage regulators and photovoltaics in unbalanced distribution systems," *IEEE Trans. Sustain. Energy*, vol. 12, no. 1, pp. 482–491, Jan. 2021.

[31] K. S. Ayyagari and N. Gatsis, "Optimal pump scheduling in multi-phase distribution networks using benders decomposition," *Electr. Power Syst. Res.*, vol. 212, Nov. 2022, Art. no. 108584.

[32] K. Mahmoud, N. Yorino, and A. Ahmed, "Optimal distributed generation allocation in distribution systems for loss minimization," *IEEE Trans. Power Syst.*, vol. 31, no. 2, pp. 960–969, Mar. 2016.

[33] L. Gan and S. H. Low, "Convex relaxations and linear approximation for optimal power flow in multiphase radial networks," in *Proc. Power Syst. Comput. Conf.*, Aug. 2014, pp. 1–9.

[34] Statista. *Best-Selling Plug-in Electric Vehicle Models Worldwide in 2021*. Accessed: Apr. 14, 2022. [Online]. Available: https://www.statista.com/statistics/960121/sales-of-all-electric-vehicles-worldwide-by-model/#main-content

[35] N. Nazir and M. Almassalkhi, "Guaranteeing a physically realizable battery dispatch without charge-discharge complementarity constraints," *IEEE Trans. Smart Grid*, vol. 14, no. 3, pp. 2473–2476, May 2021.

[36] L. Bai, J. Wang, C. Wang, C. Chen, and F. Li, "Distribution locational marginal pricing (DLMP) for congestion management and voltage support," *IEEE Trans. Power Syst.*, vol. 33, no. 4, pp. 4061–4073, Jul. 2017.

[37] K. Mahmoud and M. Lehtonen, "Comprehensive analytical expressions for assessing and maximizing technical benefits of photovoltaics to distribution systems," *IEEE Trans. Smart Grid*, vol. 12, no. 6, pp. 4938–4949, Nov. 2021.

[38] I. Alsaleh, "Comprehensive optimization models for voltage regulation in PV-rich multi-phase distribution systems," Ph.D. thesis, Dept. Elect. Eng., College Eng., Univ. South Florida, Tampa, FL, USA, 2020.

[39] M. Grant and S. Boyd. (2014). *CVX: MATLAB Software for Disciplined Convex Programming, Version 2.1*.

[40] M. C. Grant and S. P. Boyd, "Graph implementations for nonsmooth convex programs," in *Recent Advances in Learning and Control*. Cham, Switzerland: Springer, 2008, pp. 95–110.

[41] A. Mosek, "The MOSEK optimization toolbox for MATLAB manual," *Release*, vol. 9, p. 98, Nov. 2018.

IBRAHIM ALSALEH (Member, IEEE) received the B.S. degree in electrical engineering from the University of Hail, Hail, Saudi Arabia, in 2012, and the M.S. and Ph.D. degrees in electrical engineering from the University of South Florida, Tampa, FL, USA, in 2016 and 2020, respectively. He is currently an Assistant Professor with the Department of Electrical Engineering, University of Hail. His current research interests include optimization and reinforcement learning in smart power grids.

HAMOUD ALAFNAN received the B.S. degree in electrical engineering from the University of Hail, Hail, Saudi Arabia, in June 2011, the M.S. degree in electrical engineering with an emphasis in smart grids from the University of New Haven, West Haven, CT, USA, in May 2016, and the Ph.D. degree in electronic and electrical engineering with an emphasis on power system protection from the University of Bath, U.K., in February 2021. Since February 2021, he has been an Assistant Professor with the Department of Electrical Engineering, University of Hail. His research interests include smart grids, power protection systems, superconductivity, energy storage systems, and fault current limiters.

ABDULLAH ALASSAF received the B.S. degree in electrical engineering from the University of Hail, Hail, Saudi Arabia, in 2013, and the M.S. and Ph.D. degrees in electrical engineering from the University of South Florida, Tampa, FL, USA, in 2017 and 2021, respectively. He is currently an Assistant Professor with the Department of Electrical Engineering, University of Hail. His current research interest includes power system dynamics and control.

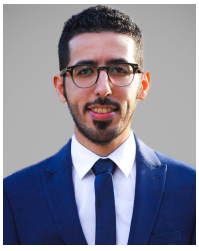

ANAS ALMUNIF (Member, IEEE) received the B.S. degree in electrical engineering from Taibah University, Saudi Arabia, in 2010, and the M.S. and Ph.D. degrees in electrical engineering from the University of South Florida, Tampa, FL, USA, in 2015 and 2019, respectively. He is currently an Assistant Professor with the Department of Electrical Engineering and the Vice Dean of Graduate Studies and Scientific Research with the College of Engineering, Majmaah University, Al Majma'ah, Riyadh, Saudi Arabia. His main research interests include power systems and renewable energy, power system monitoring and state estimation, optimization in power systems, phasor measurement unit (PMU), data identification, and system and parameter identification.